Journal of Applied Mechanics and Technical Physics, Vol. 44, No. 5, pp. 685–698, 2003

MATHEMATICAL SIMULATION OF THE MECHANISM OF ACOUSTIC DRYING OF POROUS MATERIALS

A. A. Zhilin, A. V. Fedorov, Yu. G. Korobeinikov, and V. M. Fomin

UDC 532.72; 669.015.23

A mathematical model is proposed for the description of moisture extraction during drying of materials in an acoustic field, and its asymptotic filtration approximation is analyzed. The calculated time of pressure relaxation in the specimen in the filtration model is found to be in good agreement with the calculation results obtained by solving equations of mechanics of heterogeneous media. The proposed model has solutions of the traveling acoustic wave type, which are stable in time and space, and adequately describes the initial stage of the process of acoustic drying.

Key words: *mechanics of heterogeneous media, mathematical simulation, moisture extraction, acoustic drying, stability.*

Extensive application of porous materials in chemical, construction, furniture, food, and other branches of industry turns attention of various specialists to the problem of studying mechanisms and processes in porous bodies under the action of external loads, which affect the quality and properties of materials. This class of materials includes solid chemical reagents obtained by pressing from disperse and finely disperse powders, natural materials of biological composition, e.g., wood, grain, etc.

In the present work, wood was chosen as an object of investigation. Wood is a complex polydisperse material with clearly expressed anisotropic properties. Wood contains a considerable amount of moisture necessary for vital activity of the tree. Depending on the sort, age, and cross-sectional area of the trunk, the content of moisture in a living tree can vary from 40 to 140%. The humidity of wood ω is understood as the amount of moisture normalized to the mass of absolutely dry wood M_2: $\omega = 100(M_1 - M_2)/M_2$ (M_1 is the mass of the wet wood specimen). To transform wood into a valuable building material, it should be made resistant to putrefaction, which is achieved by removing moisture.

Various methods of wood drying based on heat addition to the material being dried are used in industry [1]. Apart from the convective method of drying, there is an alternative acoustic method. In acoustic drying, moisture is removed from the material being dried by irradiation by sound with appropriate characteristics. The main advantages of acoustic drying is the high intensity of the process, the possibility of controlling it in a wide range, and reaching an almost arbitrary final humidity of wood. A principal difference of the acoustic method from the traditional one is that drying proceeds without an increase in temperature of the material being dried ("cold" drying [2]). This makes possible defect-free drying of thick beams with high strength of dry wood, which is lower in convective drying because of overheating.

The process of acoustic drying of materials has been known for a long time [3], but there is no single approach to its description. Therefore, construction of a comprehensive mathematical model that allows one to describe physical mechanisms of drying of porous materials at room temperature in a high-intensity acoustic field is an urgent problem.

Institute of Theoretical and Applied Mechanics, Siberian Division, Russian Academy of Sciences, Novosibirsk 630090. Translated from Prikladnaya Mekhanika i Tekhnicheskaya Fizika, Vol. 44, No. 5, pp. 101–116, September–October, 2003. Original article submitted March 31, 2003.

Physicomathematical Formulation of the Problem of Beam Drying in the Approximation of Mechanics of Heterogeneous Media. *Basic Equations and Formulation of the Problem of Wood Drying with Allowance for Velocity Nonequilibrium and Pressure Difference of the Phases.* We consider the problem of drying of a porous body by excitation of acoustic vibrations in the body. We study the motion of the liquid in a wooden beam of length l with an area of the rectangular cross section S. We assume that the left end of the beam is rigidly fixed ($u_2 = u_1 = 0$); the right end is free, and small rarefaction of about 0.1 atm is provided at the right butt-end face of the beam. This allows us to reduce the problem of migration of the liquid in the porous structure of the specimen to the problem of linear acoustics of mechanics of heterogeneous media. We consider the main flow with the parameters $P_i = P_0 = 1$ atm and $u_2 = u_1 = 0$ ($i = 1$ refers to the liquid and $i = 2$ to the solid skeleton).

Equations of mechanics of heterogeneous media, which take into account the difference in velocities and pressures of the components of the mixture, are used for the mathematical description of the posed problem. In the one-dimensional isothermal approximation, the problem is described by a system of differential equations that express the laws of conservation of mass and momentum for each component of the mixture, supplemented by the equation of m_2-transfer:

$$\frac{\partial \rho_1}{\partial t} + \frac{\partial \rho_1 u_1}{\partial x} = 0, \qquad \frac{\partial \rho_2}{\partial t} + \frac{\partial \rho_2 u_2}{\partial x} = 0, \qquad \frac{\partial \rho_1 u_1}{\partial t} + \frac{\partial \rho_1 u_1^2}{\partial x} = -m_1 \frac{\partial P_1}{\partial x} + F_{\mathrm{S}},$$
$$\frac{\partial \rho_2 u_2}{\partial t} + \frac{\partial \rho_2 u_2^2}{\partial x} = -m_2 \frac{\partial P_2}{\partial x} - (P_2 - P_1) \frac{\partial m_2}{\partial x} - F_{\mathrm{S}}, \qquad \frac{\partial m_2}{\partial t} + u_2 \frac{\partial m_2}{\partial x} = R. \tag{1}$$

System (1) is hyperbolic. To close the system, we supplement it by equations of state for each component and by the geometric identity:

$$P_i = a_i^2(\rho_{ii} - \rho_{ii,0}), \qquad m_1 = 1 - m_2. \tag{2}$$

In (1), (2), $\rho_i = m_i \rho_{ii}$ is the mean density of the ith component of the mixture, u_i is the velocity of the ith component, P_i is the pressure of the ith component, m_i is the volume concentration of the ith component, $F_{\mathrm{S}} = m_1 \rho_2 (u_2 - u_1)/\tau_{\mathrm{S}}$ is the Stokes force, $\tau_{\mathrm{S}} = 2\rho_{22} r^2/(9\mu_1)$ is the time of Stokes relaxation of velocities, $R = m_1 m_2 (P_2 - P_1)/\mu_2$ is a function that describes the process of transfer of the solid phase, μ_i is the dynamic viscosity of the ith component, ρ_{ii} is the true density of the ith component, a_i is the velocity of sound in the material of the ith component, $\rho_{ii,0}$ is the true density of the material of the ith component, x is the spatial variable, r is the pore radius, and t is the time.

Transition to Dimensionless Variables. To perform a parametric analysis and increase the applicability area of the results obtain, we pass to the dimensionless variables $\bar\rho_i$, $\bar u_i$, $\bar P_i$, $\bar x$, and $\bar t$. Normalization was performed with respect to physical parameters in the initial (undisturbed) state:

$$\bar\rho_i = \frac{\rho_i}{\rho_{11,0}}, \qquad \bar u_i = \frac{u_i}{a_1}, \qquad \bar P_i = \frac{P_i}{\rho_{11,0} a_1^2}, \qquad \bar x = \frac{x}{l}, \qquad \bar t = \frac{a_1 t}{l}.$$

Here l is the characteristic linear scale. In the first component, the dimensionless velocity of sound and its true density equal unity; for the second component, $a = a_2/a_1$ and $\bar\rho = \rho_{22,0}/\rho_{11,0}$, respectively.

During normalization, the right side of the equation of m_2-transfer R has the dimension $1/t$, and we can introduce a new variable τ_{m_2}, which is a function of μ_2 and describes the time of pressure relaxation of the components of the mixture. According to the estimate of [4], $\mu_2 \approx \rho_{22,0} a_2 d$; therefore, we have $\tau_{m_2} = 2a_2\rho_{22,0} r/(\rho_{11,0} a_1^2)$ in the dimensional form and $\bar\tau_{m_2} = 2a\bar\rho\,\bar r$ in the dimensionless form.

After normalization, system (1) has the same form. The expressions for the characteristic times of the processes of velocity and pressure relaxation of the components are $\bar\tau_{\mathrm{S}} = 2\bar\rho\bar r^2/(9\bar\mu_1)$ and $\bar\tau_{m_2} = 2\bar\mu_2$, and the dimensionless equations of state are

$$\bar P_1 = \bar\rho_1/\bar m_1 - 1, \qquad \bar P_2 = a^2(\bar\rho_2/\bar m_2 - \bar\rho). \tag{3}$$

In what follows, the bar over the dimensionless variables is omitted.

Linearization of the Initial System of Equations. In the linear approximation, the amplitude of vibrations is so small that we can neglect all changes caused by mass and momentum transfer. Mathematically, this is expressed in neglecting terms of Eq. (1) containing the second powers and products of small quantities determining the deviation of parameters of the mixture from the equilibrium state.

We represent the variables ρ_i, u_i, P_i, and m_i as

$$\rho_i = \rho_{i0} + \rho_i', \qquad u_i = u_{i0} + u_i', \qquad P_i = P_{i0} + P_i', \qquad m_i = m_{i0} + m_i', \tag{4}$$

where ρ_{i0}, u_{i0}, P_{i0}, and m_{i0} are constant equilibrium values of densities, velocities, pressures, and volume concentrations of the components of the mixture, and ρ_i', u_i', P_i', and m_i' are the deviations of the densities, velocities, pressures, and volume concentrations of the components from the equilibrium values. We assume that u_{i0} and P_{i0} in the equilibrium state are equal to zero.

Substituting (4) into the dimensionless analog of system (1) and the equations of state (3) and neglecting small quantities, we obtain linearized equations of mechanics of heterogeneous media for acoustic vibrations

$$\begin{gathered} \frac{\partial \rho_1'}{\partial t} + \rho_{10}\frac{\partial u_1'}{\partial x} = 0, \qquad \frac{\partial \rho_2'}{\partial t} + \rho_{20}\frac{\partial u_2'}{\partial x} = 0, \\ \rho_{10}\frac{\partial u_1'}{\partial t} + m_{10}\frac{\partial P_1'}{\partial x} = F_{\mathrm{S}}', \qquad \rho_{20}\frac{\partial u_2'}{\partial t} + m_{20}\frac{\partial P_2'}{\partial x} = -F_{\mathrm{S}}', \qquad \frac{\partial m_2'}{\partial t} = R', \end{gathered} \tag{5}$$

where $F_{\mathrm{S}}' = m_{10}\rho_{20}(u_2' - u_1')/\tau_{\mathrm{S}}$ and $R' = m_{10}m_{20}(P_2' - P_1')/\tau_{m_2}$. The equations of state (3) and the geometric identity acquire the following form:

$$P_1' = (\rho_1' - m_1')/m_{10}, \qquad P_2' = a^2(\rho_2' - m_2'\bar{\rho})/m_{20}, \qquad m_1' = -m_2'. \tag{6}$$

Below, the primes at linearized variables are omitted, and the use of nonlinearized variables is specially indicated.

Introduction of a Small Parameter. All dimensionless quantities in system (5) are small; therefore, for convenience, we consider the parameters $P_i = \varepsilon P_i^0$, $u_i = \varepsilon u_i^0$, $\rho_i = \varepsilon \rho_i^0$, and $m_i = \varepsilon m_i^0$ (ε is a small quantity). Then, P_i^0, u_i^0, ρ_i^0, and m_i^0 are finite quantities. Cancelling ε, we obtain an equation whose structure is similar to Eq. (5).

Heterogeneous Model of the Drying Process. In the present work, the heterogeneous model is understood as a mathematical model used to study drying of a porous material consisting of wood and a filler (water) filling voids in the solid material. The examined mixture of wood and water obeys the main assumptions of mechanics of heterogeneous media; therefore, the study can be performed within the model of interpenetrating continua. According to this model, each point in space is characterized by a complete set of physical parameters (density, velocity, pressure, etc.) for each phase. For each phase, we write the laws of conservation (1) or (5) represented by differential equations in partial derivatives.

For the numerical solution of system (5) with closing equations (6) and initial-boundary conditions corresponding to the physical problem, we use a modified method of "coarse particles" of the first order of approximation [5].

Since rarefaction is set at the free end of the beam in both phases $P_1^0(t) = P_2^0(t) = -1$, an unloading wave propagates inward. Figure 1 shows the pressure distribution in water and beam. At $t = 5$, the pressure in wood decreases from the initial value equal to zero to $P_2^0 \approx -0.9$; the most drastic decrease is observed in the unloading wave (segment $A'B'$ in Fig. 1b). The pressure $P_2^0 = -1$ set at the right end of the specimen is reached in the relaxation zone behind the unloading wave. The change in pressure of the liquid P_1^0 also occurs in the unloading wave, which lags behind the unloading wave in wood. Immediately behind the unloading wave front moving over the rigid skeleton (point $A'B'$ in Fig. 1a), the unloading wave in the liquid is formed. Thus, a precursor appears whose leading front propagates with the velocity of sound in the solid skeleton and the rare front propagates with the velocity of sound in the liquid. Then follows the unloading wave (segment AB in Fig. 1a) with smooth transition to the equilibrium value specified at the right end of the beam. The velocities of the unloading waves AB and $A'B'$ correspond to the velocities of disturbances in the corresponding media. With time ($t \geqslant 10$), the width of the precursor zone increases, since $a_2 > a_1$. The parameters u_i^0 behave similarly, and the amplitude of velocity in the second phase decreases with time. The velocity in the liquid is a function smoothly varying due to friction between the phases in the region between the leading shock in the solid skeleton (point $A'B'$) and the closing shock in the liquid (point AB).

Figure 2 shows the flow rate of the liquid Q_1 through the free end of the beam versus time. During 40 msec ($t = 600$), almost a constant value of velocities of the components equal to zero is established in the entire beam 5 m long, and $P_1^0 = P_2^0 = -1$. The profiles of densities of the components correspond to the pressure profiles in the respective phases.

A set of calculations of pressure in the beam with different pore diameters was performed. In Fig. 3, the points refer to the times of pressure relaxation for pores 50, 200, and 400 μm in diameter. With decreasing pore diameter, a significant increase in the time of velocity and pressure relaxation in the components is observed.

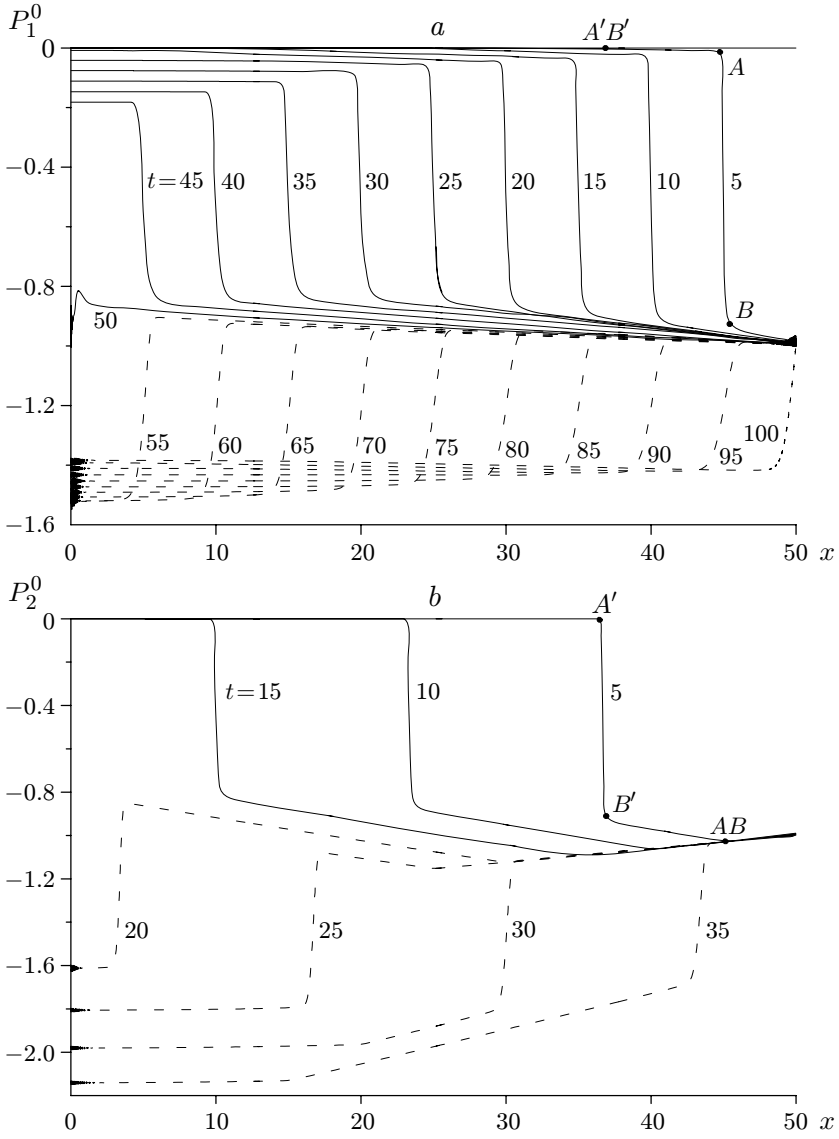

Fig. 1. Propagation of unloading waves in water (a) and wood (b): the solid curves refer to waves propagating from the free boundary to the rigid wall; the dashed curves refer to waves moving in the opposite direction.

Filtration Model of the Drying Process. *Area of Applicability of the Filtration Theory.* Let us estimate the Stokes force on the basis of the filtration theory. We write the Darcy filtration law [6] in the dimensional form

$$\boldsymbol{u} = -(k/\mu_1)\,\mathrm{grad}\,P,$$

where μ_1 is the dynamic viscosity of the filtered liquid and k is the permeability depending on the geometric parameters of the porous medium, which has the dimension of area. The permeability of most sorts of materials is low. For example, $k = 10^{-12}$–10^{-13} m^2 for coarse-grain sandstone and $k = 10^{-14}$ m^2 for compact sandstone. To evaluate the permeability coefficient for wood, we use the Kozeny–Kármán equation derived with the use of the analogy between a porous medium and a system of parallel tubes, which relates the permeability of the porous material with the porosity and specific area of the surface. According to [7], we have

$$k = d^2 m_1^3/(150(1 - m_1^2)).$$

The permeability coefficients (in Darcy; 1 Da $= 1.02 \cdot 10^{-12}$ m^2) for various volume concentrations of water and pore diameters are listed in Table 1. Note, an increase in both the pore diameter and the volume concentration of water in the specimen leads to an increase in permeability of the porous material. It follows from Table 1 that

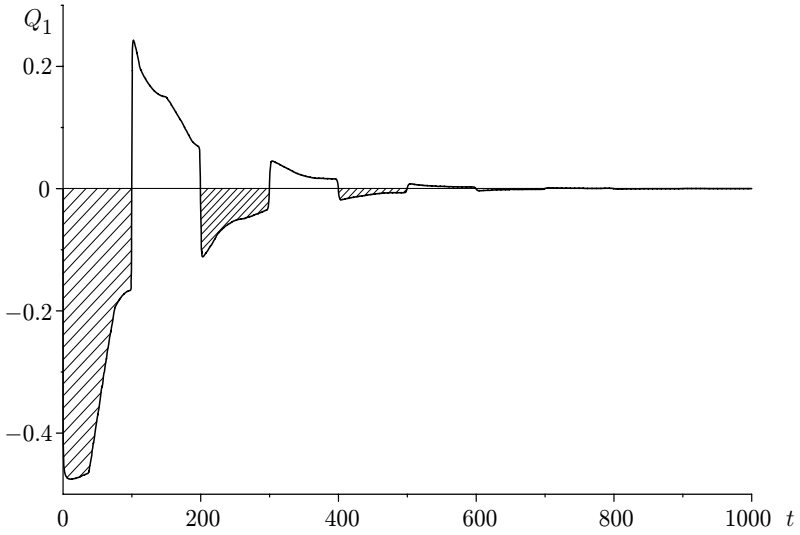

Fig. 2. Flow rate of the liquid through the free end of the beam versus time (the dashed region is the volume of the liquid leaving the specimen being dried).

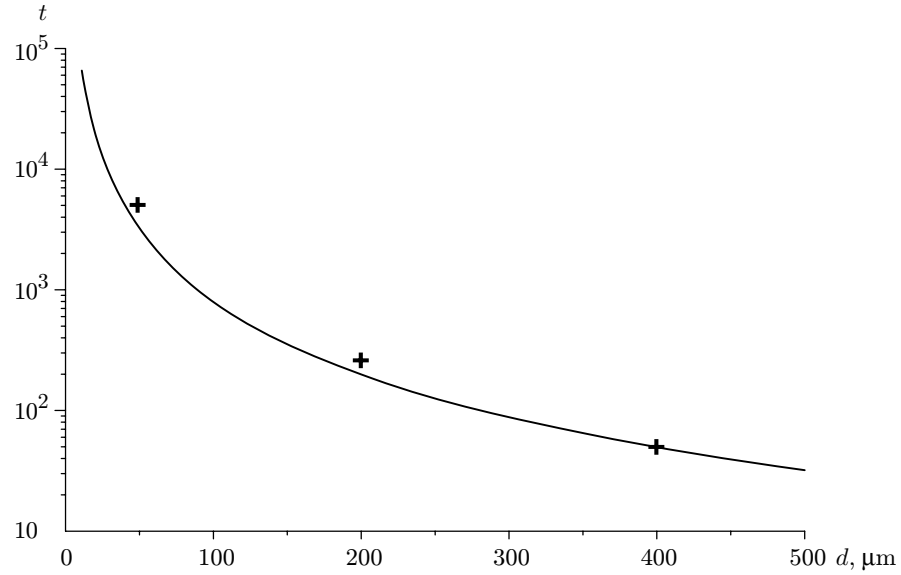

Fig. 3. Time of pressure relaxation in the beam versus the pore diameter: the solid curve shows the calculation by the filtration model, and the points show the calculation by the heterogeneous model.

the permeability of wood significantly depends on the parameters m_1 and d. For instance, if the pore diameter in the beam cross section changes from 20 to 40 μm, the permeability coefficient in this cross section can increase by a factor of 4.

In the one-dimensional approximation, the Darcy law has the form

$$u = -\frac{k}{\mu_1}\,\frac{\partial P_1}{\partial x}.$$

As the velocity u in the filtration problem, we use the mass velocity of the filtered material, i.e., $u = m_1 u_1$. Then, we have

$$\frac{\partial P_1}{\partial x} = -\frac{\mu_1 m_1 u_1}{k}. \tag{7}$$

At the same time, from the law of conservation of momentum for the light component (1), with allowance for the filtrational character of the flow, we obtain the expression

TABLE 1

d, μm	k, Da		
	$m_1 = 0.3$	$m_1 = 0.5$	$m_1 = 0.7$
10	0.01939	0.10893	0.43957
20	0.07757	0.43573	1.75830
30	0.17453	0.98039	3.95617
40	0.31028	1.74292	7.03319
50	0.48481	2.72331	10.98936
100	1.93924	10.89325	43.95745
150	4.36328	24.50980	98.90427
200	7.75695	43.57298	157.82981

$$F_{\mathrm{S}} = m_1 \frac{\partial P_1}{\partial x}. \tag{8}$$

Substituting the expression for $\partial P_1/\partial x$ from (7) into (8), we find the relation between the permeability and the Stokes force:

$$k = -\mu_1 m_1^2 u_1 / F_{\mathrm{S}}. \tag{9}$$

Since the flow is filtrational ($u_2 = 0$), the expression for the Stokes force takes the form

$$F_{\mathrm{S}} = -18\mu_1 m_1 m_2 u_1 / d^2.$$

Substituting the resultant expression into (9), we find the dependence of permeability on the particle diameter and volume concentration of the components of the mixture

$$k = m_1 d^2/(18 m_2).$$

Based on the previously found permeability of wood $k = 2 \cdot 10^{-10}$–10^{-13} m^2, we determine the particle diameter

$$d = \sqrt{18 m_2 k / m_1}.$$

Thus, we have $d = 40$–100 μm for $k = 2 \cdot 10^{-10}$ m^2 and $d = 5$–25 μm for $k = 10^{-13}$ m^2. Therefore, the approximation $C_d = 24/\,\mathrm{Re}$ (Re is the Reynolds number) is valid for pore diameters from 5 to 100 μm.

In the general case, the expression for the Stokes force also contains the Reynolds number and the drag coefficient C_d:

$$F_{\mathrm{S}} = \frac{m_1 \rho_2}{\tau_{\mathrm{S}}} C_d \frac{\mathrm{Re}}{24} (u_2 - u_1).$$

Substituting $\mathrm{Re} = \rho_1 |u_1 - u_2| d/(m_1 \mu_1)$ into the above-given relation, we obtain the expression for permeability in the form

$$k = \frac{4}{3} \frac{m_1^2 \mu_1 d}{\rho_1 m_2 u_1 C_d}.$$

Analytical Solution of the Problem of Specimen Drying. Let $u_2^0 = 0$, $P_2^0 = \mathrm{const}$, and $\partial u_1^0/\partial t \ll 1$. Then, we have $\rho_2^0 = \mathrm{const}$ and $F_{\mathrm{S}} = -m_{10}\rho_{20} u_1^0/\tau_{\mathrm{S}}$; the initial system (5) acquires the form

$$\frac{\partial \rho_1^0}{\partial t} + \rho_{10} \frac{\partial u_1^0}{\partial x} = 0, \qquad \frac{\partial P_1^0}{\partial x} = -\frac{\rho_{20} u_1^0}{\tau_{\mathrm{S}}}. \tag{10}$$

From the second equation of system (10), we find

$$u_1^0 = -\frac{\tau_{\mathrm{S}}}{\rho_{20}} \frac{\partial P_1^0}{\partial x}.$$

Substituting the resultant expression into the first equation of system (10), we obtain the equation

$$\frac{\partial P_1^0}{\partial t} = k \frac{\partial^2 P_1^0}{\partial x^2} \tag{11}$$

$[k = \rho_{10}\tau_{\mathrm{S}}/(m_{10}\rho_{20})]$ with the following initial and boundary conditions:

$$t = 0: \qquad P_1^0(x, 0) = \begin{cases} 0, & 0 \leqslant x < l, \\ -1, & x = l; \end{cases} \tag{12}$$

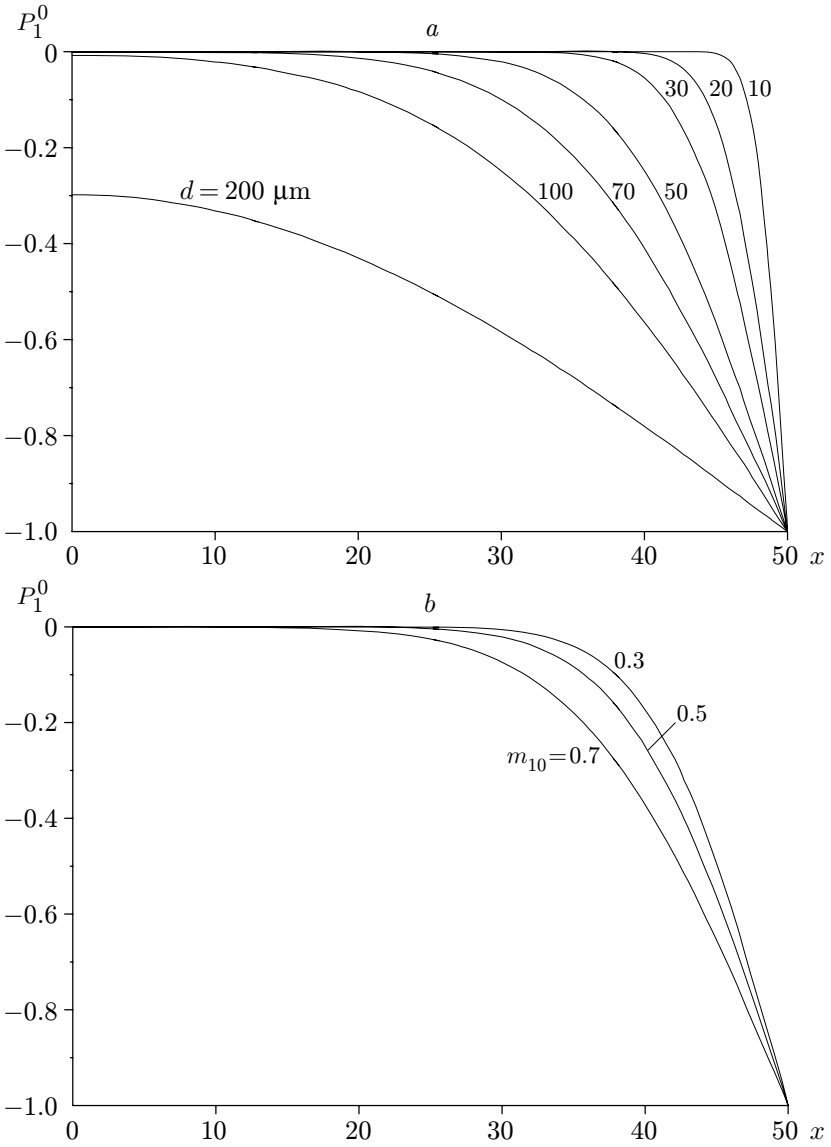

Fig. 4. Pressure in the medium as a function of the pore diameter (a) and volume concentration of water (b) in the beam for $t = 10$: $m_{10} = 0.5$ (a) and $d = 50$ μm (b).

$$x = l: \quad P_1^0(l,t) = -1, \qquad x = -l: \quad P_1^0(-l,t) = -1, \qquad x = 0: \quad \frac{\partial P_1^0(0,t)}{\partial x} = 0. \tag{13}$$

The differential equation obtained is the heat-conduction equation. To solve it, we use the method of separation of variables (Fourier method) [8]. The solution of problem (11) satisfying the boundary conditions (13) and initial conditions (12) is written as the series

$$P_1^0(x,t) = -1 + \sum_{n=1}^{\infty} \frac{4(-1)^{n+1}}{\pi(2n-1)} \cos\Big(\frac{\pi x}{2l}\,(2n-1)\Big) \exp\Big(-k\,\frac{\pi^2 t}{4l^2}\,(2n-1)^2\Big).$$

Figure 4a shows the behavior of the filtration unloading wave propagating in beams with different pore diameters. It is seen that the unloading wave velocity in the beam increases with increasing pore diameter. Figure 4b shows the pressure distributions in the liquid contained in the beam for various initial volume concentrations of water. It should be noted that the unloading wave velocity in the beam increases with increasing volume concentration of water in the material. Thus, in the course of acoustic drying of porous materials, in addition to a decrease in humidity of the beam, the velocity of acoustic waves in wood decreases, which is caused by the increase in the damping coefficient of acoustic disturbances in a dry medium.

The solid curve in Fig. 3 shows the time of pressure relaxation in the beam versus the pore diameter. The results predicted by the filtration model are in good agreement with the calculation results obtained by the heterogeneous model.

Dispersion Relations. Substituting the expressions for P_1^0 and P_2^0 from the equations of state (6) into the initial system (5), we obtain a system of differential equations for the sought functions ρ_1^0, ρ_2^0, u_1^0, u_2^0, and m_2^0:

$$\begin{gathered}
\frac{\partial \rho_1^0}{\partial t} + \rho_{10}\frac{\partial u_1^0}{\partial x} = 0, \qquad \frac{\partial \rho_2^0}{\partial t} + \rho_{20}\frac{\partial u_2^0}{\partial x} = 0,\\
\rho_{10}\,\frac{\partial u_1^0}{\partial t} + \frac{\partial \rho_1^0}{\partial x} + \frac{\partial m_2^0}{\partial x} - \frac{m_{10}\rho_{20}(u_2^0 - u_1^0)}{\tau_{\mathrm{S}}} = 0,\\
\rho_{20}\,\frac{\partial u_2^0}{\partial t} + a^2\,\frac{\partial \rho_2^0}{\partial x} - a^2\,\bar\rho\frac{\partial m_2^0}{\partial x} + \frac{m_{10}\rho_{20}(u_2^0 - u_1^0)}{\tau_{\mathrm{S}}} = 0,\\
\frac{\partial m_2^0}{\partial t} - \frac{a^2 m_{10}\rho_2^0}{\tau_{m_2}} + \frac{m_{20}\rho_1^0}{\tau_{m_2}} + \frac{(m_{20} + a^2\bar\rho m_{10})m_2^0}{\tau_{m_2}} = 0.
\end{gathered} \tag{14}$$

The solution of system (14) is sought in the form of a plane sinusoidal wave, written in an exponential form $\mathbf{\Phi} = \mathbf{\Phi}_0\,\mathrm{e}^{i(\omega t - kx)}$ [k is the wavenumber, $\omega = 2\pi/T$ is the cyclic (circular) frequency of the wave, T is the period of oscillations, and $\mathbf{\Phi} = \mathbf{\Phi}(\rho_1^0, \rho_2^0, u_1^0, u_2^0, m_2^0)$ is the vector of the solution]. By substituting this solution into (14) and cancelling $\mathrm{e}^{i(\omega t - kx)}$, we obtain a system of five linear equations for five unknowns ρ_{01}^0, ρ_{02}^0, u_{01}^0, u_{02}^0, and m_{02}^0. For this system, we write the determinant A consisting of coefficients at the corresponding unknowns:

$$A = \begin{vmatrix}
i\omega & 0 & -\rho_{10}ik & 0 & 0\\
0 & i\omega & 0 & -\rho_{20}ik & 0\\
-ik & 0 & \rho_{10}i\omega + \dfrac{m_{10}\rho_{20}}{\tau_{\mathrm{S}}} & -\dfrac{m_{10}\rho_{20}}{\tau_{\mathrm{S}}} & -ik\\
0 & -a^2ik & -\dfrac{m_{10}\rho_{20}}{\tau_{\mathrm{S}}} & \rho_{20}i\omega + \dfrac{m_{10}\rho_{20}}{\tau_{\mathrm{S}}} & a^2\bar\rho ik\\
\dfrac{m_{20}}{\tau_{m_2}} & -\dfrac{a^2 m_{10}}{\tau_{m_2}} & 0 & 0 & i\omega + \dfrac{m_{20} + a^2\bar\rho m_{10}}{\tau_{m_2}}
\end{vmatrix}.$$

To obtain dispersion relations, the determinant A is equated to zero. Substituting the expressions for $\rho_{10} = m_{10}$ and $\rho_{20} = \bar\rho m_{20}$, after simplifications, we obtain the dependence between ω and k:

$$\begin{gathered}
a^2ik^4\omega - ik^2\omega^3 - a^2ik^2\omega^3 + i\omega^5 - (k^2m_{10}\omega^2 + a^2k^2\bar\rho m_{20}\omega^2 - m_{10}\omega^4 - \bar\rho m_{20}\omega^4)/\tau_{\mathrm{S}}\\
- (a^2k^2\omega^2 m_{20} + a^2k^2\omega^2 m_{10}\bar\rho - \omega^4 m_{20} - a^2\omega^4 m_{10}\bar\rho)/\tau_{m_2} + (a^2ik^2m_{10}^2\bar\rho\omega + 2a^2ik^2m_{10}m_{20}\bar\rho\omega\\
+ a^2ik^2m_{20}^2\bar\rho\omega - i\omega^3 m_{10}m_{20} - a^2im_{10}^2\bar\rho\omega^3 - im_{20}^2\bar\rho\omega^3 - a^2im_{10}m_{20}\bar\rho^2\omega^3)/(\tau_{\mathrm{S}}\tau_{m_2}) = 0.
\end{gathered} \tag{15}$$

Grouping terms of Eq. (15) containing ω, we obtain the expression

$$i\omega^4 + \omega^3 A_1 - i\omega^2[k^2(1 + a^2) + A_2] - \omega k^2 A_3 + ia^2k^2(k^2 + A_4) = 0, \tag{16}$$

where $A_1 = (m_{10} + \bar\rho m_{20})/\tau_{\mathrm{S}} + (m_{20} + a^2\bar\rho m_{10})/\tau_{m_2}$, $A_2 = (m_{10} + \bar\rho m_{20})(m_{20} + a^2\bar\rho m_{10})/(\tau_{\mathrm{S}}\tau_{m_2})$, $A_3 = (m_{10} + a^2\bar\rho m_{20})/\tau_{\mathrm{S}} + a^2(m_{20} + \bar\rho m_{10})/\tau_{m_2}$, and $A_4 = \bar\rho/(\tau_{\mathrm{S}}\tau_{m_2})$.

The cyclic frequency of the wave can be represented as a sum of the real and imaginary parts:

$$\omega = \omega_r + i\gamma.$$

Here ω_r is the real part and γ is the growth rate of small perturbations whose sign determines flow stability (if $\gamma > 0$, the flow is stable). Substituting ω into (16), we obtain an equation that can be written as a system of two equations for the real and imaginary parts:

$$\begin{gathered}
\omega_r\{\omega_r^2(A_1 - 4\gamma) + 4\gamma^3 - 3A_1\gamma^2 + 2\gamma[k^2(1 + a^2) + A_2] - k^2A_3\} = 0,\\
\omega_r^4 - \omega_r^2[6\gamma^2 - 3A_1\gamma + k^2(1 + a^2) + A_2]\\
+ \gamma^4 - A_1\gamma^3 + [k^2(1 + a^2) + A_2]\gamma^2 - k^2A_3\gamma + a^2k^2(k^2 + A_4) = 0.
\end{gathered} \tag{17}$$

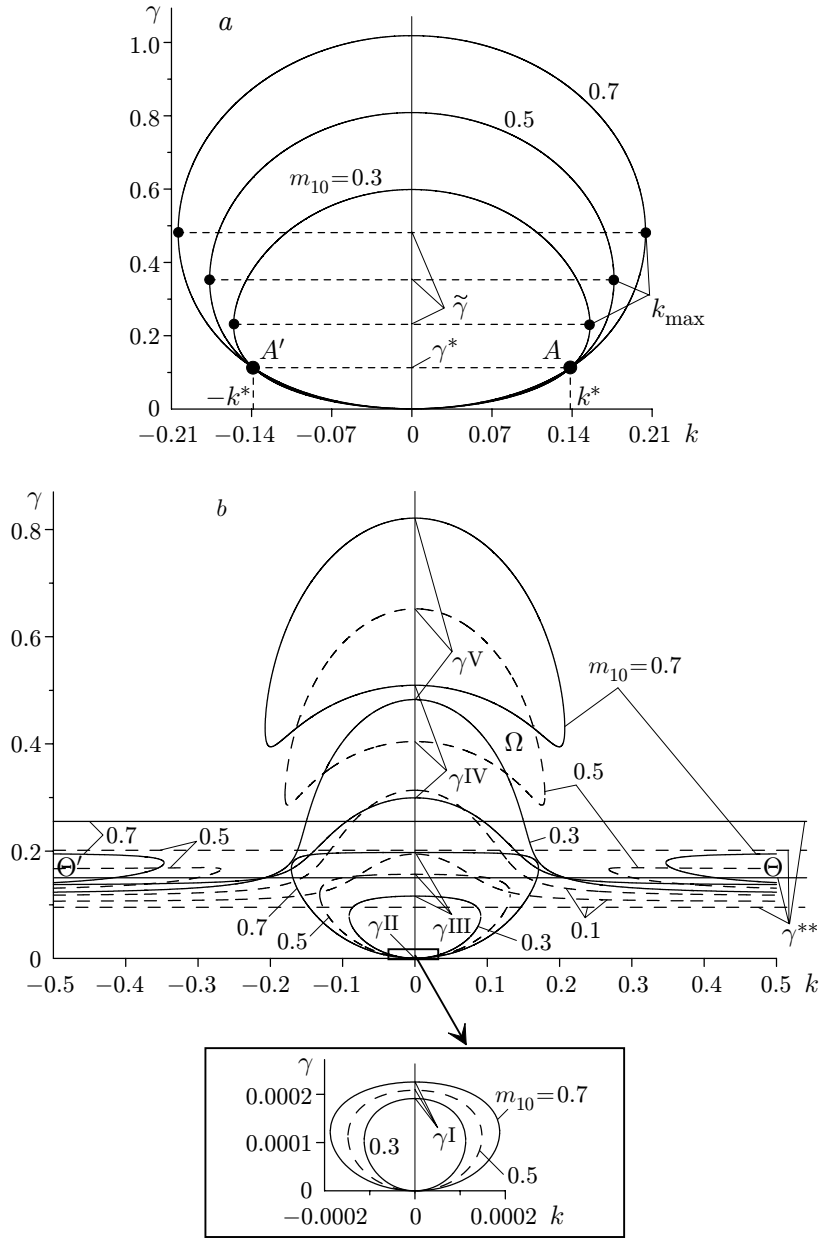

Fig. 5. Growth rate of small perturbations versus the wavenumber: the first and second solutions of system (17) are shown in Fig. 5a and 5b, respectively.

From the first equation of system (17), we can find two solutions for the real part: the trivial solution $\omega_r = 0$ and the solution in the form of a function of the growth rate of small perturbations $\omega_r^2 = \{4\gamma^3 - 3A_1\gamma^2 + 2\gamma[k^2(1+a^2) + A_2] - k^2A_3\}/(4\gamma - A_1)$. Substituting the first solution into the equation for the imaginary part, we obtain a fourth-order polynomial for determining γ with varied k and initial volume concentration of water:

$$\gamma^4 - A_1\gamma^3 + [k^2(1+a^2) + A_2]\gamma^2 - k^2A_3\gamma + a^2k^2(k^2 + A_4) = 0. \tag{18}$$

Figure 5a shows the dependence of the roots of Eq. (18) on the initial parameters. For $k = 0$, there are two multiple roots $\gamma = 0$, $\gamma^+ = (m_{10} + \bar{\rho}m_{20})/\tau_{\mathrm{S}}$ and $\gamma^- = (m_{20} + a^2\bar{\rho}m_{10})/\tau_{m_2}$, and $\gamma^- > \gamma^+$. With increasing (decreasing) k, the values of γ^- decrease to $\tilde{\gamma}$, and the values of γ^+ increase to $\tilde{\gamma}$. It is seen in Fig. 5 that the branches of the solution γ^+ and γ^- ($\gamma^+ = \gamma^- = \tilde{\gamma}$) intersect at $k = |k_{\max}|$; with further increase in $|k|$, the roots pass to the imaginary plane. Note, with increasing m_{10}, the absolute value of $k_{\max}$ and the value of $\tilde{\gamma}$ increase.

TABLE 2

m_{10}	γ^{**}	$\gamma^{\mathrm{I}} \cdot 10^{-3}$	$\gamma^{\mathrm{II}} \cdot 10^{-3}$	γ^{III}	γ^{IV}	γ^{V}
0.1	0.097	0.174	0.456	0.076	0.195	0.314
0.2	0.124	0.183	0.479	0.096	0.247	0.398
0.3	0.150	0.191	0.501	0.116	0.300	0.483
0.4	0.176	0.200	0.524	0.137	0.352	0.567
0.5	0.202	0.208	0.546	0.157	0.404	0.652
0.6	0.229	0.217	0.568	0.177	0.457	0.737
0.7	0.255	0.226	0.591	0.198	0.509	0.821
0.8	0.281	0.234	0.613	0.218	0.562	0.906
0.9	0.307	0.243	0.635	0.238	0.614	0.990

We study whether the solutions can pass from the positive half-plane to the negative one. We find the real roots of Eq. (18) for $\gamma = 0$. Since $\bar{\rho}$, τ_{S}, and τ_{m_2} are always positive, the resultant biquadratic equation with respect to k has one multiple real solution $k = 0$ and two imaginary solutions $k_{\pm} = \pm i\sqrt{\bar{\rho}/(\tau_{\mathrm{S}}\tau_{m_2})}$. Thus, all solutions of Eq. (18) are located in the upper half-plane where $\gamma > 0$ and vanish at the point $k = 0$ only.

If the second solution $\omega_r = \omega_r(\gamma, k, m_{10})$ is substituted into the equation for the imaginary part, then, for $\gamma \neq A_1/4$, the expression for the growth rate of small perturbations can be represented as a sixth-power polynomial. Being too cumbersome, this expression is not given here. The roots of this equation were found numerically and are plotted in Fig. 5b. Three types of roots can be identified. The roots of the first type are shown in Fig. 5b in an enlarged scale. They have the form of an ellipse. With increasing volume concentration of moisture, the size of the ellipse increases, and γ changes from zero to γ^{I} [in Table 2, the values of γ^i (i = I–V) for various m_{10} are listed]. The solutions of the second type have an ellipsoid shape (Fig. 5b). In our case, we have $\gamma \in [\gamma^{\mathrm{II}}, \gamma^{\mathrm{III}}]$. With increasing m_{10}, the values of the roots also increase. The roots of the third type significantly depend on the initial volume concentration of moisture in the beam (Fig. 5b). For $m_{10} = 0.7$, the solutions have the form of a closed curve Ω, which is shaped as a horseshoe and is located in the vicinity of $k = 0$, and two semi-infinite curves Θ and Θ' located symmetrically about the axis γ. The curve Ω is located higher than the horizontal line $\gamma = \gamma^{**}$ (the values of γ^{**} are determined from the expression for ω_r^2 when the denominator vanishes and are listed in Table 2), and the curve Θ is located below the line $\gamma = \gamma^{**}$. With decreasing m_{10}, the curve Ω is shifted toward the lower values of γ and gradually approaches the line $\gamma = \gamma^{**}$ (which is also shifted toward the lower values of γ with decreasing m_{10}). At the same time, the curves Θ move in the same direction as Ω but slower than the line $\gamma = \gamma^{**}$ (see the solutions for $m_{10} = 0.5$ and 0.3). Thus, with decreasing m_{10} to $m_{10}^* = (\tau_{\mathrm{S}} + \tau_{m_2}\bar{\rho})/[\tau_{\mathrm{S}}(1 + a^2\bar{\rho}) + \tau_{m_2}(1 + \bar{\rho})] = 0.17585$, the curves of the solutions Ω and Θ converge. For $m_{10} < m_{10}^*$, the curves are united and transformed into two nonintersecting curves that belong to the entire range of values of $k \in (-\infty, +\infty)$ with small variations in γ to the values γ^{IV} and γ^{V}, respectively, in the vicinity of $k = 0$ (see the solution for $m_{10} = 0.1$). Note, in this case, both curves of the solution are located above the line $\gamma = \gamma^{**}$.

We study the possibility of intersection of the axis k with the solution of the considered equation in the interval $(-\infty, +\infty)$. We assume that $\gamma = 0$ in this interval, which allows us to obtain the expression for $\omega_r^2 = -k^2 A$ and the biquadratic equation for k in the form

$$k^4(A^2 + A(1 + a^2) + a^2) + k^2\Big(A\frac{(m_{10} + \bar{\rho}m_{20})(m_{20} + a^2\bar{\rho}m_{10})}{\tau_{\mathrm{S}}\tau_{m_2}} + \frac{a^2\bar{\rho}}{\tau_{\mathrm{S}}\tau_{m_2}}\Big) = 0, \tag{19}$$

where

$$A = \Big(\frac{m_{10} + a^2\bar{\rho}m_{20}}{\tau_{\mathrm{S}}} + a^2\,\frac{m_{20} + \bar{\rho}m_{10}}{\tau_{m_2}}\Big)\Big/\Big(\frac{m_{10} + \bar{\rho}m_{20}}{\tau_{\mathrm{S}}} + \frac{m_{20} + a^2\bar{\rho}m_{10}}{\tau_{m_2}}\Big) > 0.$$

Equation (19) has two multiple trivial solutions $k = 0$ and two imaginary solutions

$$k = \pm i\sqrt{\frac{A(m_{10} + \bar{\rho}m_{20})(m_{20} + a^2\bar{\rho}m_{10}) + a^2\bar{\rho}}{\tau_{\mathrm{S}}\tau_{m_2}(A^2 + A(1 + a^2) + a^2)}}.$$

Hence, all possible solutions are located in one positive half-plane (Fig. 5b) except for the point $k = 0$ where $\gamma = 0$.

The analysis of dispersion relations shows that acoustic vibrations generated in the specimen are stable and decaying in the range of parameters (pore size, initial porosity of the specimen, etc.) obtained in experiments. From the viewpoint of efficiency of acoustic drying, it is of interest to consider regimes of excitation of oscillations in the specimen, which correspond to the closed curves shown in Fig. 5, because spatial disturbances decay weakly

in this case. Note, there exists a point A invariant for all m_{10}, where the absolute value of k^* and the value of γ^* are constant (Fig. 5a).

Dividing expression (15) by k^5, introducing the phase velocity $c = \omega/k$ corresponding to the velocity of the sinusoidal wave, and using the expressions $\tau_U = \omega\tau_{\rm S}$ and $\tau_P = \omega\tau_{m_2}$, we obtain the dispersion relation in the form

$$ic(1-c^2)(a^2-c^2) - c^3[c^2(m_{10}+\bar\rho m_{20}) - (m_{10}+a^2\bar\rho m_{20})]/\tau_U$$

$$- c^3[c^2(m_{20}+a^2 m_{10}\bar\rho) - a^2(m_{20}+m_{10}\bar\rho)]/\tau_P + ic^3[a^2\bar\rho - c^2(m_{20}+a^2\bar\rho m_{10})(m_{10}+m_{20}\bar\rho)]/(\tau_U\tau_P) = 0. \quad (20)$$

One of the solutions of Eq. (20) is a constant solution $c = 0$, which corresponds to the trivial case of the absence of propagation of sinusoidal waves in the medium.

Depending on the characteristic relaxation times, there are several types of flows of the mixture.

1. Frozen flow ($\tau_U \to \infty$ and $\tau_P \to \infty$). In this case, the velocities and pressures of the components are different, and expression (20) is transformed to

$$(1-c^2)(a^2-c^2) = 0.$$

The resultant equation has four roots corresponding to the velocities of sound in pure materials composing the mixture ($c_{1,2} = \pm 1$ and $c_{3,4} = \pm a$).

2. Equilibrium flow ($\tau_U \to 0$ and $\tau_P \to 0$). In this case, the velocities and pressures of the phases are identical, and expression (20) is reduced to the form

$$ic^2[a^2\bar\rho - c^2(m_{20}+a^2\bar\rho m_{10})(m_{10}+m_{20}\bar\rho)]/(\tau_U\tau_P) = 0.$$

This equation has also four roots: $c_{1,2} = 0$ and $c^2_{3,4} = a^2\bar\rho/[(m_{20}+a^2\bar\rho m_{10})(m_{10}+\bar\rho m_{20})]$. The second pair of the roots corresponds to the equilibrium velocity of sound represented in [9, 10] in the form

$$C^2_{\rm eq} = \frac{\xi_1}{m_1}\,\frac{m_1 C - \rho\xi_1}{m_1^2 C - \rho\xi_1}.$$

3. Equilibrium-frozen flow ($\tau_U \to 0$ and $\tau_P \to \infty$). In this case, the velocities of the components are identical, and the pressures are different ($U_1 = U_2$ and $P_1^0 \ne P_2^0$); expression (20) has the form

$$c^2[c^2(m_{10}+\bar\rho m_{20}) - (m_{10}+a^2\bar\rho m_{20})]/\tau_U = 0.$$

The solution has also two roots equal to zero and two roots of the form $c^2_{3,4} = (m_{10}+a^2\bar\rho m_{20})/(m_{10}+\bar\rho m_{20})$. The last two roots determine the equilibrium-frozen velocity of sound $C_{\rm eq,fr}$, which was used in [9, 10] in the form

$$C^2_{\rm eq,fr} = \xi_1 + a^2\xi_2.$$

4. Frozen-equilibrium flow ($\tau_U \to \infty$ and $\tau_P \to 0$). In this case, the velocities of the components are different, and the pressures are identical; Eq. (20) is reduced to the expression

$$c^2[c^2(m_{20}+a^2 m_{10}\bar\rho) - a^2(m_{20}+m_{10}\bar\rho)]/\tau_P = 0,$$

which has four roots: $c_{1,2} = 0$ and $c^2_{3,4} = a^2(m_{20}+\bar\rho m_{10})/(m_{20}+a^2\bar\rho m_{10})$. The last two roots characterize the frozen-equilibrium velocity of sound $C^2_{\rm fr,eq}$, which can be represented in the form

$$C^2_{\rm eq,fr} = C^2_{\rm eq}(m_{20}^2/\xi_2 + m_{10}^2/\xi_1).$$

Figure 6 shows the characteristic velocities of sound versus the initial volume concentration of water in the beam. The equilibrium, equilibrium-frozen, and frozen-equilibrium velocities of sound change monotonically in the interval from the velocity of sound in the liquid ($a_1 = 1$) to the velocity of sound in wood ($a_2 = a$).

Experiment. The experiments on moisture extraction from wood were performed on a model drying setup of the Institute of Theoretical and Applied Mechanics of the Siberian Division of the Russian Academy of Sciences. A built-in Gartman generator was used as a source of high-intensity sound. The operation principle of the experimental setup is described in detail in [11].

Two series of experiments were performed. The material under study in the first series was pine. The first specimen had the following dimensions: thickness $h = 21$ mm, width $b = 130$ mm, and length $l = 1003$ mm. The second specimen had the following dimensions: $h = 50$ mm, $b = 81$ mm, and $l = 1002$ mm. The wave intensity was 178 dB and its frequency was 125 Hz. The pore diameter in the specimen varied from 20 to 40 μm. The weight of the specimens was registered in the experiments (Table 3).

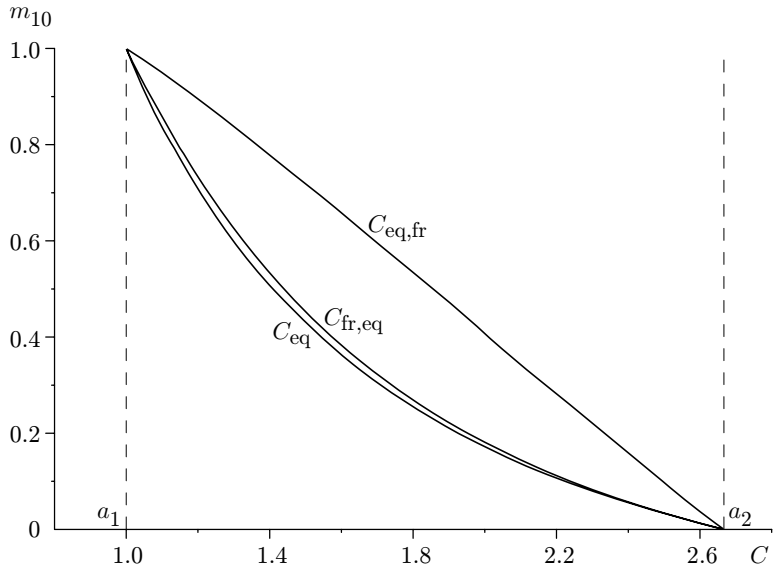

Fig. 6. Characteristic velocities of sound versus the initial volume concentration of water in the beam.

TABLE 3

t, min	Weight of specimen 1, kg	Weight of specimen 2, kg
0	2.285	3.090
5	2.265	3.075
10	2.250	3.060
15	2.235	3.050
20	2.220	3.040
25	2.205	3.025
30	2.190	3.015
35	2.180	3.005
40	2.170	3.000
45	2.160	—

TABLE 4

t, min	Specimen weight, kg			
	Specimen 1	Specimen 2	Specimen 3	Specimen 4
0	1.190	1.910	2.420	3.060
5	1.170	1.880	2.400	3.025
10	1.150	1.865	2.380	3.005
15	1.145	1.850	2.370	2.995
20	1.130	1.840	2.355	2.975
25	1.120	1.825	2.345	2.960
30	1.115	1.815	2.335	2.940

In the second series, we examined four birch specimens of identical width $b = 70$ mm and length $l = 950$ mm; the thickness was $h = 19$, 30, 40, and 50 mm for specimens 1, 2, 3, and 4, respectively. The wave intensity was 177 dB and its frequency was 130 Hz. The mean pore diameter in the specimen was 30 μm. The test results are listed in Table 4.

Comparison of Experimental and Numerical Data. In numerical calculations within the mathematical model (5), (6), we used the value of the maximum pressure amplitude $P_{\max}$ evaluated by the known intensity of the acoustic wave L (measured in decibels) in accordance with [12]: $L = 20 \log (P_{\max}/(\sqrt{2}\tilde{P}_0))$, where $\tilde{P}_0 = 2 \cdot 10^{-5}$ Pa. We obtained $P_{\max} = 22{,}467$ Pa in the first test series and $P_{\max} = 20{,}024$ Pa in the second one.

Figure 7 shows the results of calculations and the physical experiment, which characterize the intensity of moisture entrainment from the specimen being dried. As a whole, the calculated estimates are in good agreement with the experimental data. It should be noted that the theoretical dependence $\Delta m(t)$ is close to linear, whereas gradual attenuation of the moisture-entrainment rate at large times of the drying process (more than one hour) is observed. This indicates the necessity of improving the model, possibly, by taking into account weak nonlinearity and the presence of air trapped in the specimen.

Conclusions. A mathematical model is proposed for the description of phenomena of moisture transfer and extraction during drying of materials at room temperature in a high-intensity acoustic field.

Based on the assumptions of the filtration theory, the mathematical model examines its asymptotic filtration approximation and offers an analytical solution of the problem of motion of the liquid in a wooden specimen under the action of acoustic disturbances. The influence of the pore diameter and volume concentration of the liquid in the specimen on the drying process is studied.

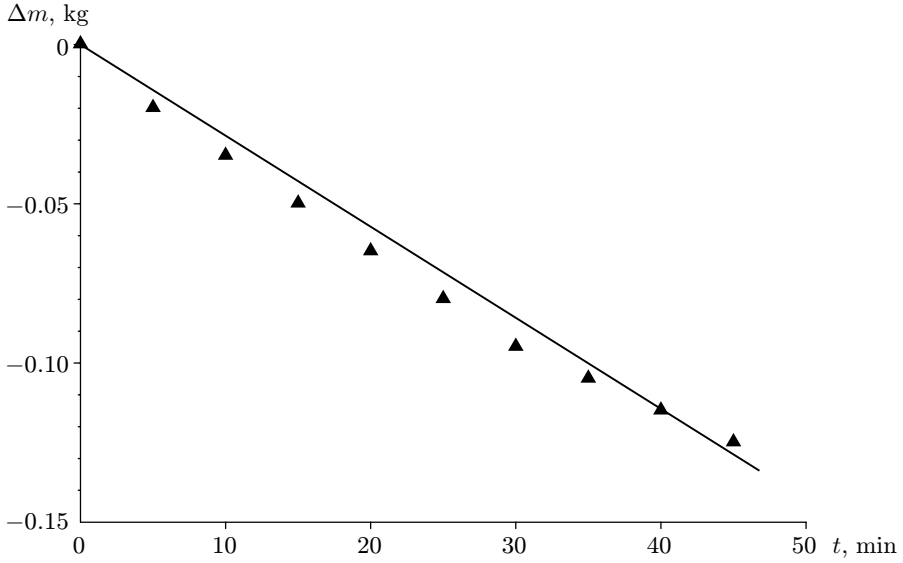

Fig. 7. Experimental (points) and calculated (solid curve) dependences of the loss of specimen weight on the drying time for pine specimen 1.

The calculation results for the time of pressure relaxation in the specimen by the filtration model are in good agreement with the calculation results obtained by solving equations of mechanics of heterogeneous media.

It is shown that, in the realistic range of parameters, the mathematical model has solutions of the traveling acoustic wave type, which are stable in time and space.

A series of experiments on moisture extraction from wood is performed, which allows obtaining integral quantitative data on drying kinetics.

It is shown that the initial stage of the process of acoustic drying can be adequately described by a simple linearized model of mechanics of heterogeneous media, which takes into account nonequilibrium velocities and pressures of the components.

The authors are grateful to Yu. A. Berezin for his assistance in this work.

This work was supported by the Foundation for supporting domestic science and within the youth grant of the Siberian Division of the Russian Academy of Sciences "Simulation of the Mechanism of Acoustic Drying" and Integration Project of the Siberian Division of the Russian Academy of Sciences (Grant No. 46).

REFERENCES

1. I. V. Krechetov, *Drying of Wood* [in Russian], Lesn. Prom., Moscow (1980).
2. V. N. Glaznev, I. V. Koptyug, and Yu. G. Korobeinikov, "Physical features of acoustic drying of wood," *Inzh.-Fiz. Zh.*, **72**, No. 3, 437–439 (1999).
3. Yu. A. Borisov and N. M. Gynkina, "Physical fundamentals of ultrasonic technology," in: *Physics and Engineering of Powerful Ultrasound* [in Russian], Book 3, Nauka, Moscow (1970), pp. 580–640.
4. M. R. Baer, R. J. Gross, J. W. Nunziato, and E. A. Igel, "An experimental and theoretical study of deflagration-to-detonation transition (DDT) in the granular explosive CP," *J. Combust. Flame,* **65**, 15–30 (1986).
5. A. A. Gubaidullin, A. I. Ivandaev, and R. I. Nigmatulin, "Modified method of coarse particles for calculating unsteady wave processes in multiphase disperse media," *Zh. Vychisl. Mat. Mat. Fiz.*, **17**, No. 6, 1531–1544 (1977).
6. G. I. Barenblat, V. M. Entov, and V. M. Ryzhik, *Theory of Unsteady Filtration of Liquid and Gas* [in Russian], Nedra, Moscow (1972).
7. S. G. Neruchev, O. B. Moiseeva, L. I. Klimova, and S. V. Smirnov, "Modeling of processes of migration and accumulation in traps," *Geolog. Geofiz.*, **41**, No. 8, 1145–1164 (2000).
8. S. K. Godunov, *Equations of Mathematical Physics* [in Russian], Nauka, Moscow (1971).

9. A. A. Zhilin, A. V. Fedorov, and V. M. Fomin, "Traveling wave in a two-velocity mixture of compressible media with different pressures," *Dokl. Ross. Akad. Nauk*, **350**, No. 2, 201–205 (1996).
10. A. A. Zhilin and A. V. Fedorov, "The shock-wave structure in a two-velocity mixture of compressible media with different pressures," *J. Appl. Mech. Tech. Phys.*, **39**, No. 2, 166–174 (1998).
11. V. N. Glaznev, Yu. G. Korobeinikov, and G. D. Kozyura, "Experimental investigation of gas-jet Gartman generators," Report No. 2308, Inst. Theor. Appl. Mech., Sib. Div., Russian Acad. of Sci., Novosibirsk (1995).
12. H. Kuchling, *Physik, Nachschlagerbucher fur Grundlagenfacher*, VEB Fachbuchverlag, Leipzig (1980).